The Xist lncRNA Exploits Three-Dimensional Genome Architecture to Spread Across the X Chromosome

Jesse M. Engreitz,[1,2] Amy Pandya-Jones,[3] Patrick McDonel,[1] Alexander Shishkin,[1] Klara Sirokman,[1] Christine Surka,[1] Sabah Kadri,[1] Jeffrey Xing,[1] Alon Goren,[1] Eric S. Lander,[1,4,5]* Kathrin Plath,[3]* Mitchell Guttman[1]*†

Many large noncoding RNAs (lncRNAs) regulate chromatin, but the mechanisms by which they localize to genomic targets remain unexplored. We investigated the localization mechanisms of the Xist lncRNA during X-chromosome inactivation (XCI), a paradigm of lncRNA-mediated chromatin regulation. During the maintenance of XCI, Xist binds broadly across the X chromosome. During initiation of XCI, Xist initially transfers to distal regions across the X chromosome that are not defined by specific sequences. Instead, Xist identifies these regions by exploiting the three-dimensional conformation of the X chromosome. Xist requires its silencing domain to spread across actively transcribed regions and thereby access the entire chromosome. These findings suggest a model in which Xist coats the X chromosome by searching in three dimensions, modifying chromosome structure, and spreading to newly accessible locations.

Mammalian genomes encode thousands of large noncoding RNAs (lncRNAs) (1–5), many of which play key functional roles in the cell (6–9). One emerging paradigm is that many lncRNAs can regulate gene expression (6, 8–11) by interacting with chromatin regulatory complexes (6, 12–14) and localizing these complexes to genomic target sites (15–17). Despite the central role of RNA-chromatin interactions, the mechanisms by which lncRNAs identify their genomic targets remain unexplored.

The Xist ncRNA provides a model to investigate the mechanisms of lncRNA localization (11, 18, 19). Xist initiates X-chromosome inactivation (XCI) by spreading in cis across the future inactive X chromosome (20, 21), recruiting polycomb repressive complex 2 (PRC2) (14, 22, 23), and forming a transcriptionally silent nuclear compartment (24, 25) enriched for repressive chromatin modifications including trimethylation of histone 3 lysine 27 (H3K27me3) (22, 23). These functions of Xist—localization to chromatin and silencing of gene expression—are mediated by distinct RNA domains (26): Transcriptional silencing requires the A-repeat domain (26), which interacts with the PRC2 chromatin regulatory complex (14), whereas localization to chromatin requires several distinct domains (26–28) and interactions with proteins associated with the nuclear matrix (29–31). Despite these advances in our understanding of Xist, we still do not understand the process by which Xist localizes to chromatin and spreads across the X chromosome.

We present a biochemical method that enables high-resolution mapping of lncRNA localization. Using this method, we explored Xist localization during initiation and maintenance of XCI. During maintenance, Xist localized broadly across the entire X chromosome, lacking focal binding sites. During initiation of XCI, Xist transferred directly from its transcription locus to distal sites across the X chromosome that are defined not by specific sequences but by their spatial proximity in the nucleus to the Xist transcription locus. Furthermore, we show that Xist initially localized to the periphery of actively transcribed regions but gradually spread across them through a mechanism dependent on the A-repeat domain. Together, these results suggest that Xist initially localizes to distal sites across the chromosome by exploiting chromosome conformation, and may spread to new sites through its ability to modify chromatin structure.

Results and Discussion

RNA Antisense Purification (RAP): A Method to Map lncRNA Interactions with Chromatin

To determine the genomic localization of lncRNAs, we developed a method termed RAP, which is conceptually similar to previous methods (32–34) in that it uses biotinylated antisense probes that hybridize to a target RNA to purify the endogenous RNA and its associated genomic DNA from cross-linked cell lysate (Fig. 1A) (35). We designed RAP to enable specific purification of chromatin associated with a target lncRNA, achieve high-resolution mapping of the associated DNA target sites upon sequencing of the captured DNA, and robustly capture any lncRNA with minimal optimization. To achieve high specificity, RAP uses 120-nucleotide antisense RNA probes to form extremely strong hybrids with the target RNA, thereby enabling purification using denaturing conditions that disrupt nonspecific RNA-protein interactions and nonspecific hybridization with RNAs or genomic DNA. RAP uses deoxyribonuclease I (DNase I) to digest genomic DNA to ~150–base pair (bp) fragments, which provides high-resolution mapping of binding sites. To robustly capture a lncRNA, RAP uses a pool of overlapping probes tiled across the entire length of the target RNA to ensure capture even in the case of extensive protein-RNA interactions, RNA secondary structure, or partial RNA degradation (supplementary text).
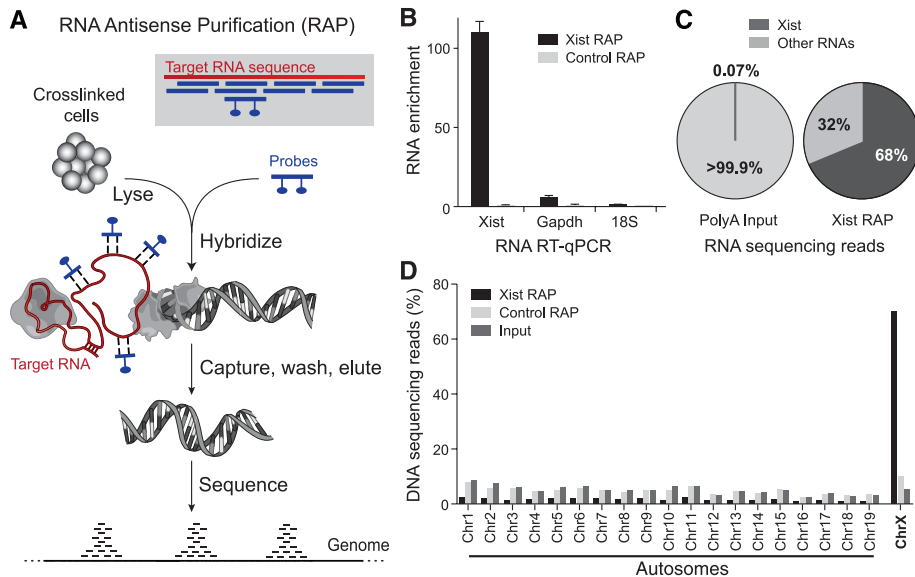
To test our method, we used RAP to purify the Xist RNA and associated DNA from female mouse lung fibroblasts (MLFs), a differentiated cell line in which Xist is expressed from and coats the inactive X chromosome. We designed antisense probes tiled every 15 nucleotides across the 17-kb Xist transcript, excluding those that showed any complementarity to other RNAs or genomic DNA regions (35). This yielded a pool of 1054 unique probes. We performed RAP and observed an enrichment of the Xist RNA by more than a factor of 100 relative to either input or a control purification using "sense" probes from the same strand as Xist itself (Fig. 1B). When we sequenced all RNAs in the purified fraction, we found that the Xist RNA constituted ~70% of alignable reads despite representing <0.1% of the polyadenylated input RNA. The remaining reads were broadly distributed across ~7500 expressed transcripts, with no single transcript exceeding 2% of the total purified RNA (Fig. 1C). We sequenced the genomic DNA that copurified with the Xist RNA and observed a strong enrichment, with >70% of the DNA sequencing reads from the Xist purification originating from the X chromosome, versus ~5% from the input DNA samples (Fig. 1D).

To ensure that the DNA purified by Xist RAP reflected the endogenous localization of Xist, we performed three control experiments (fig. S1) (35): (i) To confirm that captured chromatin reflected preexisting interactions occurring in vivo, we purified Xist from non–cross-linked cellular extracts. In this condition, we did not obtain any detectable DNA signal by quantitative polymerase chain reaction (qPCR) despite obtaining comparable enrichments of the Xist RNA (35). (ii) To rule out the possibility that RAP captured genomic DNA through nonspecific hybridization with the probes or the target RNA, we tested

Fig. 1. RNA antisense purification (RAP) accurately purifies lncRNA-chromatin interactions. (A) Schematic diagram of RAP. Biotinylated probes (blue) are hybridized to the target RNA (red) cross-linked to proteins and DNA. Gray inset: 120-nucleotide antisense capture probes are designed to tile across the entire target RNA. (**B**) Reverse transcription qPCR of the RNA captured using antisense probes to Xist (Xist RAP, black) or sense probes to Xist (control RAP, gray) in MLFs. Enrichments represent means ± SEM (*N* = 3 replicate experiments) and are normalized to the mean of the sense control experiments. Note that Tsix, an antisense transcript overlapping Xist, is not expressed in MLFs. (**C**) RNA sequencing reads originating from the Xist transcript (dark gray) and all other cellular RNAs (light gray) for polyA-selected RNA (left) and RNA captured using antisense probes for the Xist RNA (right) (*35*). (**D**) DNA sequencing reads aligning to each chromosome after purification with antisense probes (Xist RAP, black), sense probes (control RAP, light gray), and input genomic DNA (dark gray) in MLFs.

whether sites with higher enrichment in Xist RAP showed complementarity to sequences present in the probes or Xist RNA sequence (*35*). We observed no relationship between sequence homology and RNA localization either on the X chromosome or on autosomes (fig. S2). (iii) To further exclude the possibility of direct probe-DNA interactions, we examined DNA captured in a control purification with sense probes that should capture double-stranded DNA with the same efficiency but will not hybridize to the target RNA. Using the sense probes, we observed no enriched regions across the entire genome (Fig. 1D) with the sole exception of a low-level enrichment at the *Xist* locus itself (*35*), likely reflecting perfect hybridization with the RNA probes. However, the amount of Xist genomic DNA purified in the control was <5% of the amount in the Xist purification, which suggests that most of the signal in Xist RAP resulted from RNA-mediated interactions (supplementary text).

Together, these results demonstrate the specificity of the RAP method to capture RNA interactions with chromatin.

Xist Binds Across the Inactive X in Differentiated Female Cells

Using RAP, we explored the localization of Xist in MLFs. We found that Xist showed enrichment over the entire X chromosome as opposed to showing punctate enrichment at specific loca-

tions (Fig. 2, A to C, and fig. S3). Indeed, >95% of 10-kb windows on the X chromosome were enriched by more than a factor of 10 relative to the input. In comparison, not a single window on an autosome reached this enrichment level (Fig. 2C). This broad localization pattern contrasts sharply with the roX2 ncRNA in *Drosophila*, which, despite its similar function of regulating gene expression across an entire chromosome, binds at discrete sites (*32*, *33*).

Although Xist showed enrichment across the entire X chromosome (factor of 23 average enrichment), we observed differences in the precise levels of enrichment across the chromosome (Fig. 2A), which were highly reproducible between replicates (Pearson correlation = 0.94; fig. S4) (*35*). To characterize this variation, we correlated Xist enrichment with other genomic features (table S1). We found that Xist enrichment strongly correlated with H3K27me3 across the entire chromosome (Pearson correlation = 0.69; Fig. 2, A and B), consistent with the known role for Xist in the recruitment of PRC2 (*14*, *22*, *23*). Xist levels also showed a strong correlation with gene density (Pearson correlation = 0.44) and a negative correlation with the density of long interspersed nuclear element (LINE) repeats (Pearson correlation = –0.25), which tend to reside in gene-poor regions.

To further explore this variation, we examined the most enriched (by a factor of >30) and least enriched (by a factor of <15) regions of the

X chromosome (Fig. 2C) (*35*). The most enriched regions showed higher H3K27me3 occupancy in MLFs (factor of 1.7) and higher gene density (factor of 3) relative to the chromosome average, consistent with the chromosome-wide correlations. The least enriched regions contained genes known to escape XCI (*36*). Consistent with their preferential positioning outside of the Xist domain (*37*, *38*), escape genes displayed a ~50% reduction in Xist occupancy relative to silenced X-chromosome genes, with the level of Xist enrichment roughly reflecting the previously reported ratio of expression from the inactive versus active X chromosome (Pearson correlation = –0.66; Fig. 2D) (*35*, *39*). Closer examination of Xist localization at some escape genes revealed sharp boundaries separating escaped and non-escaped domains (Fig. 2E). One of the least enriched regions resided immediately distal to the *Xist* locus and included the lncRNA genes *Jpx* and *Ftx*, both of which have been previously reported to escape XCI and act as positive regulators of Xist (*40*, *41*) (Fig. 2F).

Together, the least enriched regions contained 53 genes with more than 40% depletion for Xist relative to the chromosome average (table S2). Twenty-four of these genes have been previously reported to partially escape inactivation, including 10 microRNA genes (*42*) and three lncRNAs (table S2). Three of these genes represent novel candidate escape genes in MLF, displaying on average 50% depletion of Xist relative to other genes on the X chromosome. The remaining genes are not expressed in MLF or are located within 300 kb of a known escape gene and thus likely do not escape XCI in this cell type.

Thus, the Xist RNA localizes broadly across the entire inactive X chromosome in differentiated cells, preferentially localizing at gene-rich regions (*43*, *44*) but excluding genes that are expressed on the inactive X chromosome. This broad localization pattern suggests that Xist localizes to chromatin in a degenerate fashion, possibly through interactions with the nuclear matrix (*29*, *30*, *44*).

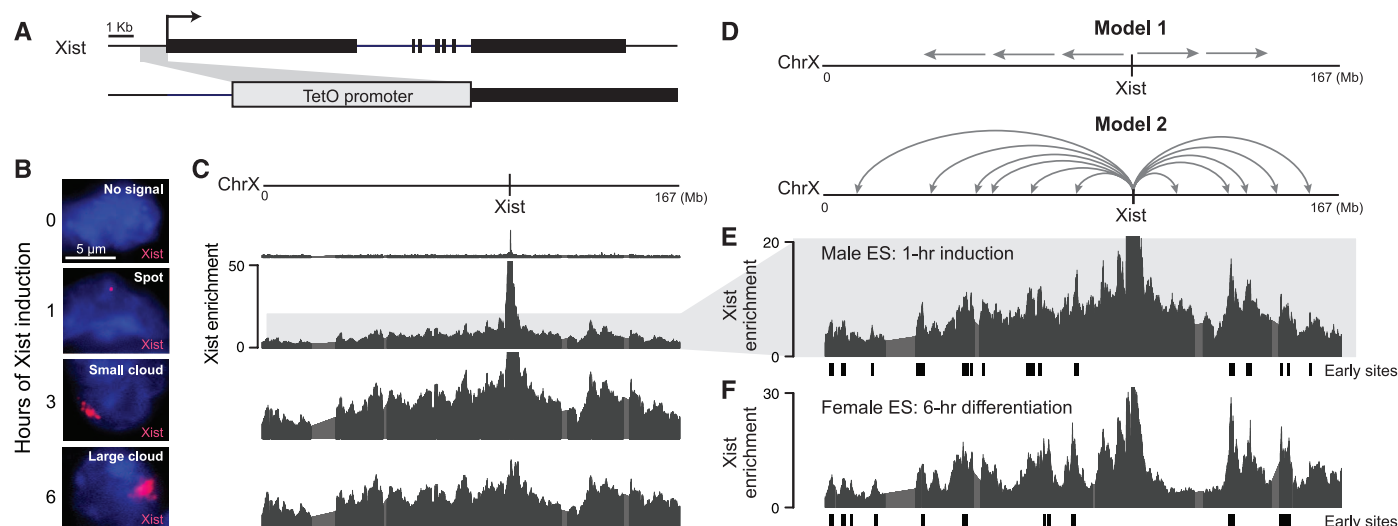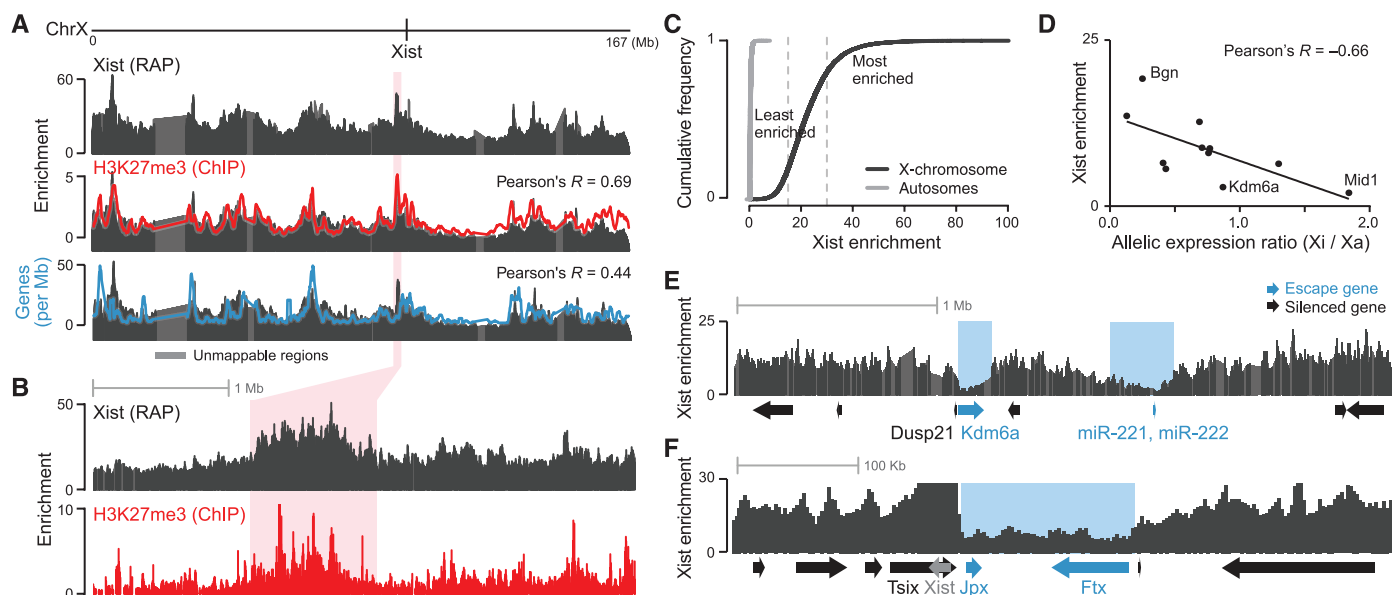### Xist Initially Localizes to Defined Regions Across the X Chromosome

To gain insight into how Xist establishes this broad localization pattern during the initiation of XCI, we examined Xist localization upon activation in mouse embryonic stem (ES) cells (*20*). In the pluripotent state, Xist is not expressed and both X chromosomes are active (*20*, *21*, *45*, *46*). Induction of differentiation triggers Xist activation on one allele, leading to the silencing of the X chromosome in cis (*20*, *21*, *45*). To synchronize the initiation of XCI, we engineered a tetracycline-inducible promoter to drive Xist expression from its endogenous locus in a male mouse ES cell line (Fig. 3A and fig. S5) (*35*). Upon induction with doxycycline, these cells increased Xist expression by a factor of ~120 over a period of 6 hours (fig. S6). RNA fluorescence in situ hybridization

(FISH) showed that after 1 hour of induction, Xist appeared as a strong focal point and grew to a characteristic cloud over time (Fig. 3B and fig. S6), accompanied by exclusion of RNA polymerase II and accumulation of PRC2 and H3K27me3 over the Xist RNA compartment (fig. S6). Cells expressing Xist concurrently si-

lenced expression of the Tsix RNA, which negatively regulates Xist in ES cells (fig. S6) (47).

To observe the process by which Xist initially spreads across the X chromosome, we used RAP to generate high-resolution maps of Xist localization across five time points from 0 to 6 hours after Xist induction (Fig. 3C and fig. S7). After

1 hour of Xist induction, we observed a strong ~5-Mb peak centered at the *Xist* transcription locus, corresponding to the spot of Xist localization observed using RNA FISH (Fig. 3B and fig. S6). Over the time course, this peak declined while Xist levels across the chromosome increased. These patterns mirrored the emergence of the

Fig. 2. High-resolution mapping of Xist localization on the inactive X chromosome in differentiated female cells. (**A**) Xist enrichment over input (dark gray), H3K27me3 enrichment over input (red line), and gene density (blue line) (35) across the entire X chromosome in female MLFs. (**B**) Zoom in on a highly enriched Xist region (light red box, chrX:95,000,000–99,000,000) shows Xist (black) and H3K27me3 (red) enrichments. (**C**) Cumulative distribution plot comparing Xist enrichment across all 10-kb windows on the X chromosome

(black) and on autosomes (gray). Dashed lines demarcate the least and most highly enriched regions on the X chromosome. (**D**) Correlation between Xist enrichment and the ratio of expression from the inactive X (Xi) and active X (Xa) for known escape genes (39). (**E**) Xist enrichment (chrX:17,031,000–19,901,000) across two of the least enriched regions (blue boxes). (**F**) Xist enrichment around the *Xist* genomic locus including one of the least enriched regions (blue box). Xist enrichment at the *Xist* locus (gray arrow) extends above the *y*-axis maximum.

Fig. 3. High-resolution view of Xist spreading during initiation of XCI. (**A**) We replaced the 1027 bases upstream of Xist with a tetracycline-responsive (TetO) promoter in male mouse ES cells (35). (**B**) Representative FISH images for the Xist RNA (red) and (DAPI) staining of the nucleus (blue) after Xist induction with doxycycline. Xist FISH signals were classified into categories—including no signal, spot, small cloud, and large cloud—at each time point (35). (**C**) Xist RAP enrichments over input across the X chromosome for the same time points as in

(B). The *y*-axis scale (0 to 50) is the same for all time points. Xist enrichment at the *Xist* locus extends above *y*-axis maximum. (**D**) Two proposed models for Xist spreading (gray arrows) from its transcription locus (tick mark) across the chromosome. (**E**) A zoom in on the *y* axis of Xist enrichment after 1 hour of Xist induction. (**F**) Xist enrichments from RAP in wild-type female ES cells after 6 hours of differentiation. Early sites are defined by significant deviations (P < 0.05) above the local (10-Mb) average (35).
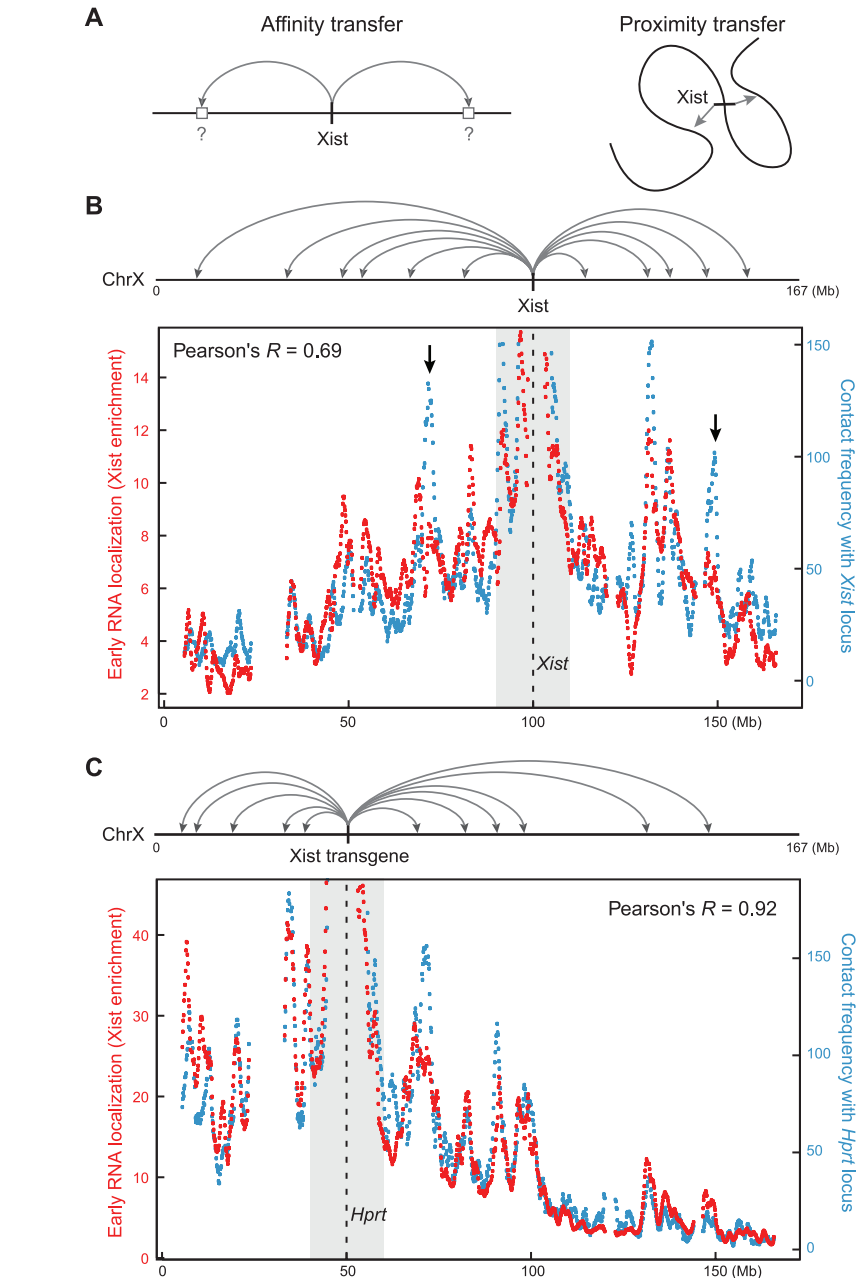
large Xist cloud observable by FISH at these time points. By 6 hours, the pattern of Xist localization began to resemble stable XCI in MLFs, where Xist localizes broadly across the X chromosome and is preferentially enriched at gene-dense regions (fig. S7).

Two models have been proposed to explain how Xist accomplishes this rapid spreading across the entire X chromosome (Fig. 3D) (*44*, *48*): Either Xist spreads uniformly from its transcription site until it coats the entire chromosome, or Xist first localizes to "early" sites that are far from the Xist transcription locus (*44*). To distinguish between these models, we examined Xist localization by RAP after 1 hour of Xist induction. We identified 28 distal sites of Xist occupancy across the chromosome ($P < 0.05$; Fig. 3E) (*35*). These sites comprised broad domains (average size 367 kb) that were concentrated in 15 regions spaced across the entire X chromosome. These sites initially showed an approximate doubling of enrichment relative to neighboring regions, but this enrichment decreased over time (Fig. 3C), which suggests that Xist preferentially localizes to these sites early during the initiation of XCI. We also performed the RAP experiment across a differentiation time course in wild-type female ES cells (fig. S8) (*35*). We found that Xist localized to these same distal sites across the X chromosome in female ES cells (Fig. 3F and figs. S7 and S9), demonstrating that Xist also targets these early sites in a normal developmental context. Thus, Xist initially transfers from its transcription locus to distal early localization sites to initiate spreading across the X chromosome.

Three-Dimensional Chromosome Conformation Guides Xist to Early Localization Sites

To determine how Xist identifies and targets these early localization sites, we considered two possible explanations (Fig. 4A): (i) Early sites may have higher affinity for the Xist RNA, enabling them to recruit Xist as it diffuses away from its transcription locus ("affinity transfer") (*48–51*). (ii) Alternatively, early sites may be defined not by affinity for Xist RNA but by spatial proximity to the site of Xist transcription ("proximity transfer") (*44*, *49*).

We first explored the affinity transfer model. Early sites were not enriched for specific sequence motifs that could play a role in recruiting Xist (*35*). We further compared Xist enrichment to >250 genomic annotations, including features such as repeat element density and chromatin immunoprecipitation sequencing experiments in ES cells (table S1) (*35*). We did not observe a significant relationship between Xist localization and LINE1 repeat elements (Pearson correlation = −0.17) (supplementary text). Instead, Xist early localization sites displayed modest enrichments (factor of <2) for gene density (table S3). Yet the chromosome-wide correlation between Xist localization and gene density was relatively modest (Pearson correlation = 0.34) (*35*), which suggests that gene

density alone does not explain early Xist localization patterns.

In the proximity transfer model (Fig. 4A), the early Xist localization sites would be in close spatial proximity to the *Xist* transcription locus before Xist RNA induction, allowing direct trans-

fer upon transcription of Xist RNA from its genomic locus to linearly distant chromosomal regions. To test this hypothesis, we examined the conformation of the X chromosome using a previously published male mouse ES cell data set (*52*) generated by genome-wide chromosome

Fig. 4. Early Xist localization correlates with the three-dimensional proximity contacts of the Xist transcription locus. (**A**) Two models for how Xist spreads to early initiation sites (marked by gray arrows in all panels). Gray boxes on the left model represent hypothetical high-affinity interaction sites. (**B**) Correlation between Xist RNA localization (red) after 1 hour of Xist induction and Hi-C contact frequencies (blue) between distal sites and the *Xist* genomic locus (dashed line). Black arrows point to selected regions with lower Xist RNA enrichments than would be expected from the Hi-C contact frequencies. (**C**) Correlation between Xist transgene RNA localization (red) after 3 hours of induction of the Xist cDNA transgene in the *Hprt* locus and Hi-C contact frequencies (blue) between distal sites and the *Hprt* integration locus (dashed line). Correlation calculations exclude the shaded gray regions (10 Mb on each side). Contact frequencies represent normalized Hi-C interaction counts in male ES cells between each window and the window containing the *Xist* or *Hprt* locus (*35*).

conformation capture [Hi-C (*53*)]. Because of the sparseness of the Hi-C contact maps, we binned the data into 1-Mb regions based on the distance from the *Xist* genomic locus (*35*). We found a strong correlation between Xist RNA localization across the X chromosome and the frequency at which distal sites contact the *Xist* genomic locus (Pearson correlation = 0.69; Fig. 4B). We note that this correlation is not driven by the strong peak in both data sets centered at the *Xist* genomic locus because we considered only sites farther than 10 Mb from *Xist* itself (*35*). This strong correlation was also observed upon differentiation of female ES cells (Pearson correlation = 0.69; fig. S10A). These correlations exceeded that of any of the >250 genomic annotations that we tested in ES cells (table S1).

One possible explanation for this correlation is that RAP might be capturing distal sites because of their proximity-mediated contacts with the *Xist* DNA locus, rather than interactions with the Xist RNA. This is possible because in Xist RAP the *Xist* DNA locus is enriched by a factor of ~10 relative to the rest of the X chromosome (Fig. 4B). By capturing the *Xist* DNA locus through purification of Xist RNA, we might indirectly enrich other distal sites that are crosslinked to the *Xist* DNA locus, thereby yielding a pattern of enrichment similar to a standard chromosome conformation capture assay. However, if we observed a similar correlation between early Xist localization and chromosome conformation in the absence of a strong localization peak at the *Xist* genomic locus, then the pattern of Xist enrichment across the chromosome cannot be explained by proximity-induced crosslinking effects. To test this, we used our inducible system to turn off Xist transcription after 1 hour of induction and profiled Xist localization (*35*). We found that Xist RNA enrichment at its DNA locus declined from a factor of 102 to a factor of 14 over input, showing a level comparable to the rest of the X chromosome (fig. S10B). Xist remained enriched at the same distal regions (figs. S7 and S9) and showed a comparable correlation with proximity contacts to the *Xist* DNA locus (Pearson correlation = 0.59; fig. S10C). We conclude that the Xist RNA interacts directly with these spatially proximal sites.

Although these data show that early Xist localization correlates with spatial proximity, they do not demonstrate a causal relationship between Xist localization and chromosome conformation. If initial Xist localization is controlled by proximity-mediated contact with the *Xist* genomic locus, then altering the conformational context of the *Xist* transcription locus should lead to an early localization pattern defined by the proximity contacts of the new integration site. To test this directly, we used a male ES cell line that expresses an Xist cDNA from a Tet-inducible transgene incorporated at the *Hprt* locus, a genomic locus ~50 Mb proximal to the endogenous *Xist* locus (*26*) (figs. S7 and S10D). When we examined these cells at early time

points after induction, we found that early Xist localization correlated strongly with proximity contacts at the *Hprt* integration site (Pearson correlation = 0.92; Fig. 4C) but not with those at the endogenous *Xist* locus (Pearson correlation = −0.02). Although these results do not exclude the possibility that additional chromatin features may be important for creating a permissive environment for Xist RNA localization, it is clear that chromosome conformation plays a dominant role in determining the early localization sites of the Xist RNA on the X chromosome.

Thus, spatial proximity to the Xist transcription locus guides early Xist RNA localization. This proximity-guided search may explain several of our other observations about Xist localization: (i) Because Xist is actively transcribed, it will be located within the "active compartment" of the nucleus (*53*). This may explain our observations that Xist preferentially localizes to gene-rich regions. (ii) Because chromosome conformation is heterogeneous in a cell population (*54*, *55*), the precise order by which Xist spreads to distal sites is likely to differ between individual cells. This may explain why Xist shows low-level early enrichment across the entire X chromosome, as all regions of the chromosome may contact the *Xist* genomic locus at some low frequency.

Xist Spreading to Active Genes Depends on Its Silencing Domain

Although early Xist localization correlated strongly with proximity contact frequency across the chromosome, we noticed several large chromosomal domains where Xist occupancy was lower than would be expected on the basis of observed proximity contacts (e.g., black arrows in Fig. 4B). These depleted regions contained many genes that are actively transcribed in ES cells; we termed these "active gene-dense regions." In contrast, the early-enriched Xist localization sites were also gene-dense but were enriched for genes that are inactive in ES cells. The depleted regions neighbored the early Xist localization sites such that Xist accumulated on the periphery of active gene-dense regions (fig. S11A).

To test whether actively transcribed genes generally showed reduced Xist occupancy, we explored Xist localization across all genes on the X chromosome 3 hours after Xist induction. Indeed, Xist showed on average a 15% focal depletion over active genes (P = 0.006, Mann-Whitney test), but was not depleted across inactive genes (Fig. 5, A and B). The level of Xist occupancy across active genes roughly reflected the level of expression in ES cells, with highly transcribed genes showing the lowest Xist occupancy (Pearson correlation = −0.33; fig. S11B). Furthermore, this focal depletion across active genes was temporary: Xist enrichment at genes expressed in ES cells increased over time and, upon stable inactivation in MLFs, was comparable to neighboring intergenic regions and inactive genes (fig. S11C). Together, these results suggest that the initial localization of Xist is
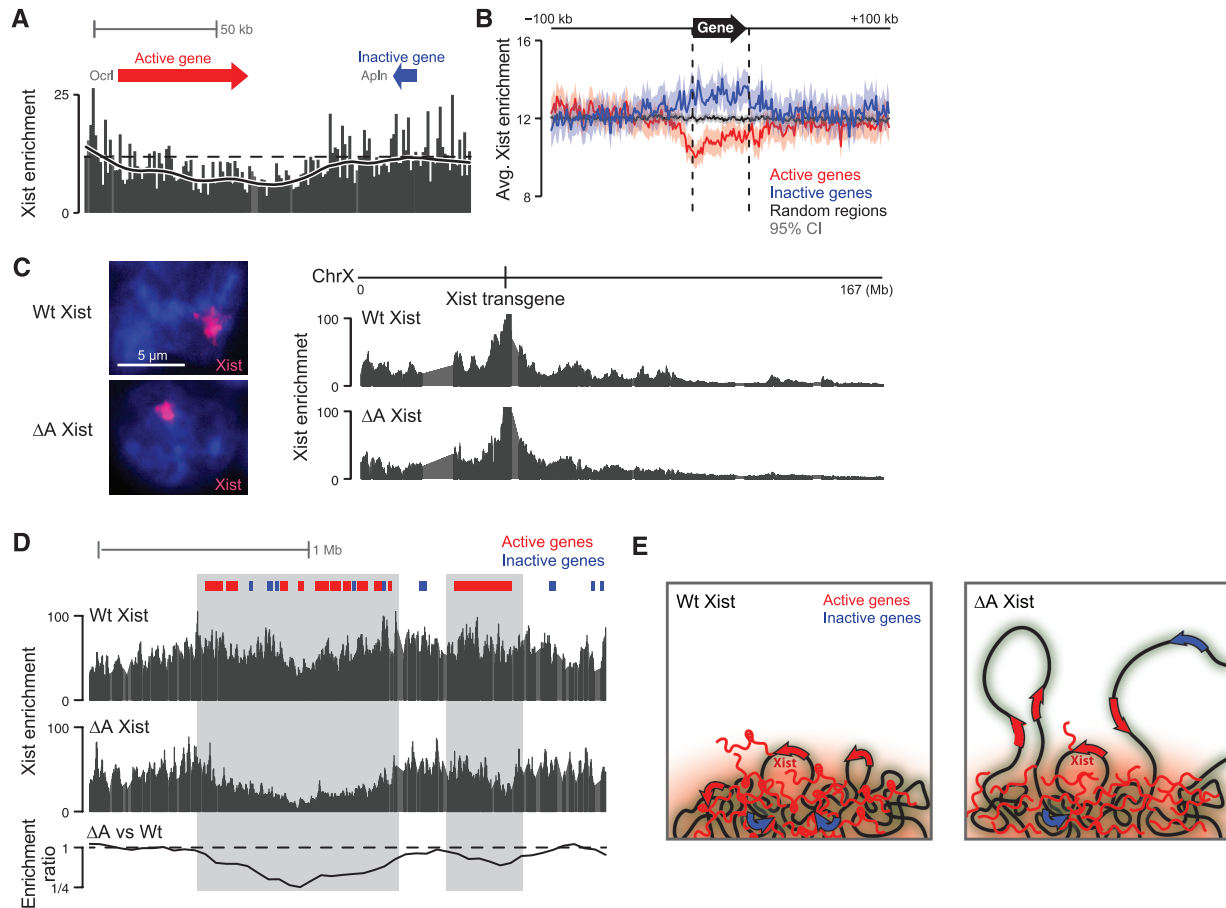
hindered by some feature of actively transcribed genes but that Xist can eventually overcome this barrier to spread across these regions.

We hypothesized that the ability of Xist to spread across active genes is dependent on its ability to silence gene expression. Previous genetic studies have identified the A-repeat within Xist as an RNA domain that is necessary for silencing gene expression but is not required for the formation of the Xist RNA compartment (*25*, *26*). We therefore repeated the RAP experiments using an Xist RNA in which the A-repeat had been deleted (ΔA Xist) (*26*). We found that the localization of ΔA Xist over the whole X chromosome looked broadly comparable to that of wild-type Xist (Fig. 5C and fig. S12), consistent with previous observations by FISH (*25*, *26*). However, at high resolution, we observed a factor of ~2 depletion for ΔA Xist occupancy relative to wild-type Xist over active gene-dense regions, with ΔA Xist instead accumulating on the edges of these regions (Fig. 5C and fig. S11, D and E). This depletion extended across the entire region including active and inactive genes as well as intergenic sequences; this finding suggests that active gene-dense regions may loop out of the ΔA Xist compartment such that even inactive genes remain physically inaccessible to ΔA Xist spreading (Fig. 5E).

These results demonstrate that Xist initially localizes to the periphery of active gene-dense regions through a mechanism independent of its A-repeat domain, but requires the A-repeat to efficiently spread across active genes and access these regions. Notably, the A-repeat domain interacts with the PRC2 chromatin-modifying complex (*14*) and enables the spatial repositioning of active genes into the Xist compartment (*25*). Together, these observations suggest that the A-repeat may allow Xist to access and spread across active gene-dense regions by modifying chromatin and altering chromosome architecture to reposition these regions into the Xist compartment (Fig. 5E).

A Model for How Xist Exploits and Alters Three-Dimensional Genome Architecture to Spread Across the X Chromosome

Our data suggest a model for how Xist can integrate its two functions—localization to DNA and silencing of gene expression—to exploit and alter nuclear architecture to spread across the X chromosome (Fig. 6). In this model, at the initiation XCI, Xist exploits the preexisting three-dimensional conformation of the X chromosome to search for target sites across the chromosome. Upon encountering a new site, Xist transfers to this region through a mechanism that allows it to localize to any region of the X chromosome, possibly through its interaction with proteins in the nuclear matrix (*29–31*). Initially, Xist accumulates at spatially proximal sites on the periphery of active gene-dense regions, positioning itself to silence neighboring genes. Through the A-repeat domain, Xist leads to transcriptional si-

Fig. 5. The A-repeat deletion of Xist cannot spread over the active regions of the X chromosome. (**A**) Xist enrichment over representative genes at chrX:45,252,000–45,408,000. Dashed line denotes the average enrichment for the entire region. Solid line represents the smoothed enrichment in sliding windows across the region. (**B**) Xist enrichment averaged over all active genes (red line, N = 608), inactive genes (blue line, N = 595), and randomly permuted regions across the X chromosome (black line) (35). Shaded regions represent 95% confidence intervals for the average enrichment. (**C**) Localization of wild-type Xist (Wt Xist, top) and Xist lacking the A-repeat (ΔA Xist, bottom) by RNA FISH (left) and RAP (right) across the X chromosome. (**D**) Comparison of Wt and ΔA Xist enrichment across a representative region at

chrX:44,600,000-47,100,000. Gray boxes mark regions that are depleted for Xist localization in ΔA versus Wt Xist. All panels present data from 3 hours after Xist induction in undifferentiated male ES cells, where Xist is expressed from its endogenous locus [(A) and (B)] or from the *Hprt* locus [(C) and (D)]. Genes were classified as active or inactive using RNA sequencing data from undifferentiated male ES cells (35). (**E**) Model: In the presence of the A-repeat (left), Xist localizes across the entire X chromosome (red cloud) but is initially excluded from active genes (red arrows). In the absence of the A-repeat (right), Xist accumulates on the periphery of active gene-dense regions but cannot spread to actively transcribed genes (red arrows) or inactive genes (blue arrows) that lie within these regions.

lencing (26) and repositioning of these genes into the growing Xist silenced compartment (25), possibly through recruitment of PRC2 (14) and other proteins (56) that lead to chromosomal compaction (57, 58). By repositioning previously active regions into its growing compartment, Xist effectively pulls new regions of active chromatin closer to the *Xist* transcription locus, thus allowing Xist RNA to spread to new sites by proximity transfer. Because Xist is actively transcribed throughout XCI, it will remain spatially close to other actively transcribed genes (59), the precise targets required for propagating Xist-mediated silencing. This process—involving searching in three dimensions, modifying chromatin state and chromosome architecture, and spreading to newly accessible locations—would explain how Xist can silence the entire X chromosome reproducibly, such that silencing occurs in each cell, even though chromosome conformation (and thus the early Xist

localization sites) may vary among individual cells in a population.

This coordinated interplay between lncRNA localization and chromosome conformation may have broader implications beyond Xist. Other lncRNAs may similarly take advantage of chromosome conformation to identify target sites in close spatial proximity (9, 17, 60), which could even reside on other chromosomes (61, 62). This search strategy capitalizes on the ability of a lncRNA to act while tethered to its transcription locus (63), in contrast to an mRNA, which requires export and translation to carry out its function. Because chromosome conformation is nonrandom, a proximity-guided search strategy might explain how low-abundance lncRNAs can reliably identify their genomic targets. Upon binding these targets, lncRNAs may in turn alter chromosome conformation through their interactions with various chromatin regulatory complexes (15, 16).
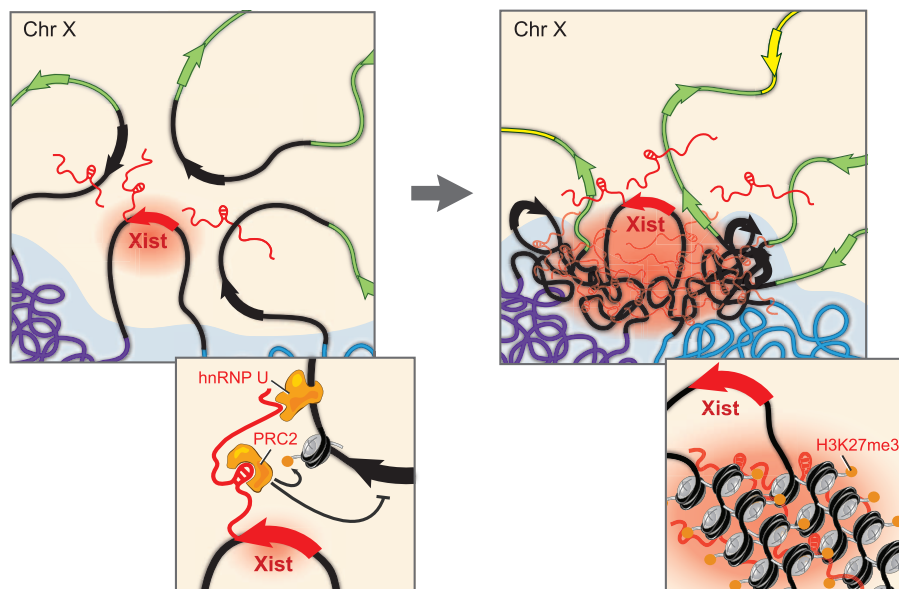
These alterations would allow localization to and regulation of previously inaccessible chromatin domains, and might even establish local nuclear compartments that contain the co-regulated targets of lncRNA complexes.

Methods

RAP

We designed a set of 120-nucleotide oligos tiled every 15 nucleotides across the entire Xist RNA sequence, excluding sequences that originated from a repetitive region. We synthesized this pool of oligos using microarray-based DNA synthesis technology and incorporated T7 promoter sequences through PCR. We generated RNA probes by in vitro transcription in the presence of biotin–uridine triphosphate. We cross-linked cells with 2 mM disuccinimidyl glutarate for 45 min and 3% formaldehyde for 10 min. We lysed cells and digested chromatin to 100- to 300-bp frag-

Fig. 6. A model for how Xist exploits and alters three-dimensional genome architecture to spread across the X chromosome. Upon induction of expression in ES cells (left), Xist (red) spreads to spatially proximal sites on the periphery of active gene-dense regions (black). Gene-poor regions (blue, purple) contact the *Xist* transcription locus infrequently, leading to slower spreading to these regions. When encountering a new region (left inset), Xist interacts with chromatin through a degenerate localization mechanism, possibly through the matrix protein hnRNP U (*30, 34*), and uses its A-repeat domain to spread over active genes. Xist may then recruit PRC2 (*14*) and other proteins (*56*) to modify and compact chromatin, thereby repositioning nearby chromosomal regions into the Xist RNA compartment (red cloud, right inset). These structural changes may propagate Xist spreading (right) by pulling new regions (green, yellow) of the chromosome into closer proximity to the *Xist* genomic locus and the growing Xist compartment.

ments through a combination of sonication and treatment with TURBO DNase. We diluted the lysate to hybridization conditions containing 3 M guanidine thiocyanate. We precleared lysate preparations by adding streptavidin-coated magnetic beads for 20 min at 45°C. Biotin-labeled RNA capture probes were mixed with the heated lysate and incubated at 45°C for 2 hours. We captured the probe-RNA complexes with streptavidin-coated beads and washed six times at 45°C. We eluted captured chromatin complexes and reversed cross links by adding proteinase K to the probe-bead complexes and incubating overnight at 65°C. We generated standard Illumina sequencing libraries and obtained >5 million 25-bp paired-end reads per sample.

Inducible Xist Cell Lines

For the time course, we used a male ES cell line in which the wild-type *Xist* promoter was replaced with a Tet-inducible promoter. For chromosome conformation and A-repeat deletion experiments, we used male ES cell lines carrying a wild-type or ΔA Xist cDNA transgene in the *Hprt* locus under control of a Tet-inducible promoter. To induce Xist expression, we added doxycycline to a final concentration of 2 μg/ml at a defined time before fixing cells.

Data Analysis

Sequencing reads were aligned to the *Mus musculus* genome (mm9). We calculated enrich-ment ratios between read counts in the RAP experiment and the input in overlapping windows across the chromosome. To identify early sites in the time-course experiments, we looked for 100-kb windows with enrichments that exceeded the local mean ($P < 0.05$). We correlated Xist enrichment across the chromosome with normalized Hi-C interaction counts measured in male mouse ES cells at 1-Mb resolution (*52*). For Hi-C correlation analysis, we excluded all bins within 10 Mb on either side of the *Xist* transcription locus, which would otherwise dominate the correlation calculation because of the strong local peaks in both the Hi-C and RAP data sets. To define active and inactive genes, we analyzed RNA sequencing data from embryonic stem cells and defined "active" genes as those expressed with $P < 0.001$.

Complete materials and methods are available as supplementary materials.

References and Notes

1. T. Derrien *et al.*, The GENCODE v7 catalog of human long noncoding RNAs: Analysis of their gene structure, evolution, and expression. *Genome Res.* **22**, 1775–1789 (2012). doi: 10.1101/gr.132159.111; pmid: 22955988
2. FANTOM Consortium, RIKEN Genome Exploration Research Group and Genome Science Group (Genome Network Project Core Group), The transcriptional landscape of the mammalian genome. *Science* **309**, 1559–1563 (2005). doi: 10.1126/science.1112014; pmid: 16141072
3. M. Guttman *et al.*, Ab initio reconstruction of cell type–specific transcriptomes in mouse reveals the conserved multi-exonic structure of lincRNAs. *Nat. Biotechnol.* **28**, 503–510 (2010). doi: 10.1038/nbt.1633; pmid: 20436462
4. M. Guttman *et al.*, Chromatin signature reveals over a thousand highly conserved large non-coding RNAs in mammals. *Nature* **458**, 223–227 (2009). doi: 10.1038/nature07672; pmid: 19182780
5. M. N. Cabili *et al.*, Integrative annotation of human large intergenic noncoding RNAs reveals global properties and specific subclasses. *Genes Dev.* **25**, 1915–1927 (2011). doi: 10.1101/gad.17446611; pmid: 21890647
6. M. Guttman *et al.*, lincRNAs act in the circuitry controlling pluripotency and differentiation. *Nature* **477**, 295–300 (2011). doi: 10.1038/nature10398; pmid: 21874018
7. I. Ulitsky, A. Shkumatava, C. H. Jan, H. Sive, D. P. Bartel, Conserved function of lincRNAs in vertebrate embryonic development despite rapid sequence evolution. *Cell* **147**, 1537–1550 (2011). doi: 10.1016/j.cell.2011.11.055; pmid: 22196729
8. U. A. Ørom *et al.*, Long noncoding RNAs with enhancer-like function in human cells. *Cell* **143**, 46–58 (2010). doi: 10.1016/j.cell.2010.09.001; pmid: 20887892
9. K. C. Wang *et al.*, A long noncoding RNA maintains active chromatin to coordinate homeotic gene expression. *Nature* **472**, 120–124 (2011). doi: 10.1038/nature09819; pmid: 21423168
10. J. L. Rinn *et al.*, Functional demarcation of active and silent chromatin domains in human HOX loci by noncoding RNAs. *Cell* **129**, 1311–1323 (2007). doi: 10.1016/j.cell.2007.05.022; pmid: 17604720
11. J. T. Lee, Epigenetic regulation by long noncoding RNAs. *Science* **338**, 1435–1439 (2012). doi: 10.1126/science.1231776; pmid: 23239728
12. M. C. Tsai *et al.*, Long noncoding RNA as modular scaffold of histone modification complexes. *Science* **329**, 689–693 (2010). doi: 10.1126/science.1192002; pmid: 20616235
13. T. Nagano *et al.*, The Air noncoding RNA epigenetically silences transcription by targeting G9a to chromatin. *Science* **322**, 1717–1720 (2008). doi: 10.1126/science.1163802; pmid: 18988810
14. J. Zhao, B. K. Sun, J. A. Erwin, J. J. Song, J. T. Lee, Polycomb proteins targeted by a short repeat RNA to the mouse X chromosome. *Science* **322**, 750–756 (2008). doi: 10.1126/science.1163045; pmid: 18974356
15. M. Guttman, J. L. Rinn, Modular regulatory principles of large non-coding RNAs. *Nature* **482**, 339–346 (2012). doi: 10.1038/nature10887; pmid: 22337053
16. J. L. Rinn, H. Y. Chang, Genome regulation by long noncoding RNAs. *Annu. Rev. Biochem.* **81**, 145–166 (2012). doi: 10.1146/annurev-biochem-051410-092902; pmid: 22663078
17. A. Kanhere, R. G. Jenner, Noncoding RNA localisation mechanisms in chromatin regulation. *Silence* **3**, 2 (2012). doi: 10.1186/1758-907X-3-2; pmid: 22292981
18. C. Gontan, I. Jonkers, J. Gribnau, Long noncoding RNAs and X chromosome inactivation. *Prog. Mol. Subcell. Biol.* **51**, 43–64 (2011). doi: 10.1007/978-3-642-16502-3_3; pmid: 21287133
19. D. Umlauf, P. Fraser, T. Nagano, The role of long non-coding RNAs in chromatin structure and gene regulation: Variations on a theme. *Biol. Chem.* **389**, 323–331 (2008). doi: 10.1515/BC.2008.047; pmid: 18225988
20. K. Plath, S. Mlynarczyk-Evans, D. A. Nusinow, B. Panning, Xist RNA and the mechanism of X chromosome inactivation. *Annu. Rev. Genet.* **36**, 233–278 (2002). doi: 10.1146/annurev.genet.36.042902.092433; pmid: 12429693
21. P. Avner, E. Heard, X-chromosome inactivation: Counting, choice and initiation. *Nat. Rev. Genet.* **2**, 59–67 (2001). doi: 10.1038/35047580; pmid: 11253071
22. K. Plath *et al.*, Role of histone H3 lysine 27 methylation in X inactivation. *Science* **300**, 131–135 (2003). doi: 10.1126/science.1084274; pmid: 12649488
23. J. Silva *et al.*, Establishment of histone h3 methylation on the inactive X chromosome requires transient recruitment of Eed-Enx1 polycomb group complexes. *Dev. Cell* **4**, 481–495 (2003). doi: 10.1016/S1534-5807(03)00068-6; pmid: 12689588

24. C. M. Clemson, J. A. McNeil, H. F. Willard, J. B. Lawrence, XIST RNA paints the inactive X chromosome at interphase: Evidence for a novel RNA involved in nuclear/chromosome structure. *J. Cell Biol.* **132**, 259–275 (1996). doi: 10.1083/jcb.132.3.259; pmid: 8636206

25. J. Chaumeil, P. Le Baccon, A. Wutz, E. Heard, A novel role for Xist RNA in the formation of a repressive nuclear compartment into which genes are recruited when silenced. *Genes Dev.* **20**, 2223–2237 (2006). doi: 10.1101/gad.380906; pmid: 16912274

26. A. Wutz, T. P. Rasmussen, R. Jaenisch, Chromosomal silencing and localization are mediated by different domains of Xist RNA. *Nat. Genet.* **30**, 167–174 (2002). doi: 10.1038/ng820; pmid: 11780141

27. C. E. Senner et al., Disruption of a conserved region of Xist exon 1 impairs Xist RNA localisation and X-linked gene silencing during random and imprinted X chromosome inactivation. *Development* **138**, 1541–1550 (2011). doi: 10.1242/dev.056812; pmid: 21389056

28. A. Beletskii, Y. K. Hong, J. Pehrson, M. Egholm, W. M. Strauss, PNA interference mapping demonstrates functional domains in the noncoding RNA Xist. *Proc. Natl. Acad. Sci. U.S.A.* **98**, 9215–9220 (2001). doi: 10.1073/pnas.161173098; pmid: 11481485

29. Y. Hasegawa et al., The matrix protein hnRNP U is required for chromosomal localization of Xist RNA. *Dev. Cell* **19**, 469–476 (2010). doi: 10.1016/j.devcel.2010.08.006; pmid: 20833368

30. D. Pullirsch et al., The Trithorax group protein Ash2l and Saf-A are recruited to the inactive X chromosome at the onset of stable X inactivation. *Development* **137**, 935–943 (2010). doi: 10.1242/dev.035956; pmid: 20150277

31. R. Agrelo et al., SATB1 defines the developmental context for gene silencing by Xist in lymphoma and embryonic cells. *Dev. Cell* **16**, 507–516 (2009). doi: 10.1016/j.devcel.2009.03.006; pmid: 19386260

32. C. Chu, K. Qu, F. L. Zhong, S. E. Artandi, H. Y. Chang, Genomic maps of long noncoding RNA occupancy reveal principles of RNA-chromatin interactions. *Mol. Cell* **44**, 667–678 (2011). doi: 10.1016/j.molcel.2011.08.027; pmid: 21963238

33. M. D. Simon et al., The genomic binding sites of a noncoding RNA. *Proc. Natl. Acad. Sci. U.S.A.* **108**, 20497–20502 (2011). doi: 10.1073/pnas.1113536108; pmid: 22143764

34. P. D. Mariner et al., Human Alu RNA is a modular transacting repressor of mRNA transcription during heat shock. *Mol. Cell* **29**, 499–509 (2008). doi: 10.1016/j.molcel.2007.12.013; pmid: 18313387

35. See supplementary materials on *Science* Online.

36. J. B. Berletch, F. Yang, J. Xu, L. Carrel, C. M. Disteche, Genes that escape from X inactivation. *Hum. Genet.* **130**, 237–245 (2011). doi: 10.1007/s00439-011-1011-z; pmid: 21614513

37. S. Dietzel et al., The 3D positioning of ANT2 and ANT3 genes within female X chromosome territories correlates with gene activity. *Exp. Cell Res.* **252**, 363–375 (1999). doi: 10.1006/excr.1999.4635; pmid: 10527626

38. G. N. Filippova et al., Boundaries between chromosomal domains of X inactivation and escape bind CTCF and lack CpG methylation during early development. *Dev. Cell* **8**, 31–42 (2005). doi: 10.1016/j.devcel.2004.10.018; pmid: 15669143

39. F. Yang, T. Babak, J. Shendure, C. M. Disteche, Global survey of escape from X inactivation by RNA-sequencing in mouse. *Genome Res.* **20**, 614–622 (2010). doi: 10.1101/gr.103200.109; pmid: 20363980

40. D. Tian, S. Sun, J. T. Lee, The long noncoding RNA, Jpx, is a molecular switch for X chromosome inactivation.

Cell **143**, 390–403 (2010). doi: 10.1016/j.cell.2010.09.049; pmid: 21029862

41. C. Chureau et al., Ftx is a non-coding RNA which affects Xist expression and chromatin structure within the X-inactivation center region. *Hum. Mol. Genet.* **20**, 705–718 (2011). doi: 10.1093/hmg/ddq516; pmid: 21118898

42. R. Song et al., Many X-linked microRNAs escape meiotic sex chromosome inactivation. *Nat. Genet.* **41**, 488–493 (2009). doi: 10.1038/ng.338; pmid: 19305411

43. S. M. Duthie et al., Xist RNA exhibits a banded localization on the inactive X chromosome and is excluded from autosomal material in cis. *Hum. Mol. Genet.* **8**, 195–204 (1999). doi: 10.1093/hmg/8.2.195; pmid: 9931327

44. A. Tattermusch, N. Brockdorff, A scaffold for X chromosome inactivation. *Hum. Genet.* **130**, 247–253 (2011). doi: 10.1007/s00439-011-1027-4; pmid: 21660507

45. S. Arthold, A. Kurowski, A. Wutz, Mechanistic insights into chromosome-wide silencing in X inactivation. *Hum. Genet.* **130**, 295–305 (2011). doi: 10.1007/s00439-011-1002-0; pmid: 21567178

46. D. H. Kim, Y. Jeon, M. C. Anguera, J. T. Lee, X-chromosome epigenetic reprogramming in pluripotent stem cells via noncoding genes. *Semin. Cell Dev. Biol.* **22**, 336–342 (2011). doi: 10.1016/j.semcdb.2011.02.025; pmid: 21376830

47. J. T. Lee, N. Lu, Targeted mutagenesis of Tsix leads to nonrandom X inactivation. *Cell* **99**, 47–57 (1999). doi: 10.1016/S0092-8674(00)80061-6; pmid: 10520993

48. S. F. Pinter et al., Spreading of X chromosome inactivation via a hierarchy of defined Polycomb stations. *Genome Res.* **22**, 1864–1876 (2012). doi: 10.1101/gr.133751.111; pmid: 22948768

49. H. Marks et al., High-resolution analysis of epigenetic changes associated with X inactivation. *Genome Res.* **19**, 1361–1373 (2009). doi: 10.1101/gr.092643.109; pmid: 19581487

50. Y. Jeon, J. T. Lee, YY1 tethers Xist RNA to the inactive X nucleation center. *Cell* **146**, 119–133 (2011). doi: 10.1016/j.cell.2011.06.026; pmid: 21729784

51. E. Heard et al., Methylation of histone H3 at Lys-9 is an early mark on the X chromosome during X inactivation. *Cell* **107**, 727–738 (2001). doi: 10.1016/S0092-8674(01)00598-0; pmid: 11747809

52. J. R. Dixon et al., Topological domains in mammalian genomes identified by analysis of chromatin interactions. *Nature* **485**, 376–380 (2012). doi: 10.1038/nature11082; pmid: 22495300

53. E. Lieberman-Aiden et al., Comprehensive mapping of long-range interactions reveals folding principles of the human genome. *Science* **326**, 289–293 (2009). doi: 10.1126/science.1181369; pmid: 19815776

54. J. Dekker, M. A. Marti-Renom, L. A. Mirny, Exploring the three-dimensional organization of genomes: Interpreting chromatin interaction data. *Nat. Rev. Genet.* **14**, 390–403 (2013). doi: 10.1038/nrg3454; pmid: 23657480

55. T. Misteli, The concept of self-organization in cellular architecture. *J. Cell Biol.* **155**, 181–185 (2001). doi: 10.1083/jcb.200108110; pmid: 11604416

56. R. S. Nozawa et al., Human inactive X chromosome is compacted through a PRC2-independent SMCHD1-HBiX1 pathway. *Nat. Struct. Mol. Biol.* **20**, 566–573 (2013). doi: 10.1038/nsmb.2532; pmid: 23542155

57. A. Rego, P. B. Sinclair, W. Tao, I. Kireev, A. S. Belmont, The facultative heterochromatin of the inactive X chromosome has a distinctive condensed ultrastructure.

J. Cell Sci. **121**, 1119–1127 (2008). doi: 10.1242/jcs.026104; pmid: 18334550

58. C. Naughton, D. Sproul, C. Hamilton, N. Gilbert, Analysis of active and inactive X chromosome architecture reveals the independent organization of 30 nm and large-scale chromatin structures. *Mol. Cell* **40**, 397–409 (2010). doi: 10.1016/j.molcel.2010.10.013; pmid: 21070966

59. E. Splinter et al., The inactive X chromosome adopts a unique three-dimensional conformation that is dependent on Xist RNA. *Genes Dev.* **25**, 1371–1383 (2011). doi: 10.1101/gad.633311; pmid: 21690198

60. P. G. Maass et al., A misplaced lncRNA causes brachydactyly in humans. *J. Clin. Invest.* **122**, 3990–4002 (2012). doi: 10.1172/JCI65508; pmid: 23093776

61. A. Williams, C. G. Spilianakis, R. A. Flavell, Interchromosomal association and gene regulation in trans. *Trends Genet.* **26**, 188–197 (2010). doi: 10.1016/j.tig.2010.01.007; pmid: 20236724

62. C. G. Spilianakis, M. D. Lalioti, T. Town, G. R. Lee, R. A. Flavell, Interchromosomal associations between alternatively expressed loci. *Nature* **435**, 637–645 (2005). doi: 10.1038/nature03574; pmid: 15880101

63. J. T. Lee, Lessons from X-chromosome inactivation: Long ncRNA as guides and tethers to the epigenome. *Genes Dev.* **23**, 1831–1842 (2009). doi: 10.1101/gad.1811209; pmid: 19684108

Supplementary Materials

www.sciencemag.org/cgi/content/full/science.1237973/DC1
Materials and Methods
Supplementary Text
Figs. S1 to S14
Tables S1 to S6
References (64–79)

Science

The Xist lncRNA Exploits Three-Dimensional Genome Architecture to Spread Across the X Chromosome

Jesse M. Engreitz, Amy Pandya-Jones, Patrick McDonel, Alexander Shishkin, Klara Sirokman, Christine Surka, Sabah Kadri, Jeffrey Xing, Alon Goren, Eric S. Lander, Kathrin Plath and Mitchell Guttman

Understanding Xist-ance

Large noncoding RNAs (lncRNAs) are increasingly appreciated to play important roles in the cell. A number of lncRNAs act to target chromatin regulatory complexes to their sites of action. **Engreitz *et al.*** (p. 10.1126/science.1237973, published online 4 July; see the Perspective by **Dimond and Fraser**) found that the mouse Xist lncRNA, which initiates X-chromosome inactivation, was transferred from its site of transcription to distant sites on the X chromosome purely through their close three-dimensional proximity to the *Xist* gene. Xist initially localized to the periphery of active genes on the X chromosome but gradually spread across them using its A-repeat domain, until the Xist RNA bound broadly across the inactive X chromosome in differentiated female cells.

ARTICLE TOOLS	http://science.sciencemag.org/content/341/6147/1237973
SUPPLEMENTARY MATERIALS	http://science.sciencemag.org/content/suppl/2013/07/03/science.1237973.DC1
RELATED CONTENT	http://science.sciencemag.org/content/sci/341/6147/720.full
REFERENCES	This article cites 78 articles, 24 of which you can access for free http://science.sciencemag.org/content/341/6147/1237973#BIBL
PERMISSIONS	http://www.sciencemag.org/help/reprints-and-permissions